EVS27
Barcelona, Spain, November 17-20, 2013

Acoustic Characteristics Concerning Construction and Drive of Axial-flux Motors for Electric Bicycles

Ming-Hung Lu[1], Ming Une Jen
[1]*Industrial Technology Research Institute,*
Bldg. 58, 195, Section 4, Chung Hsing Rd.,Chutung, Hsinchu, Taiwan, minghung-lu@itri.org.tw

Abstract

Ride quality, including perceptible noise and tactile vibration, is one of key considerations for electric bicycles. Featured with high torque density and slim shape, axial-flux permanent magnet (AFPM) motors fulfill most of the integration requirements for electric bicycles. Such a pancake shape construction, however, is prone to structural vibration since large axial force exerts on the stator by the rotor magnets. In this study, two conventional bicycles were modified to equip with either inrunner or outrunner AFPM motors, and induced noise concerns during riding. Measured data of phase currents, vibration and noise were analyzed by time signature, spectrum or cepstrum for both motors. Additional modal testing was performed for the outrunner motor as structural resonances occurred. Through investigations both on the motor structure and the motor drive, the major vibration and noise peaks were correlated to their excitation sources. In this study, the torque ripple induced by current control scheme was the root cause of the inrunner motor noise. The outrunner motor noise was mainly caused by the stator slotting effect and the coincidence with structural resonance. Moreover, the perceptibility of switching noise was highly linked to pulse-width-modulation switching frequency. After the comprehensive cause-effect analysis and effective remedies to refine the drive scheme or the controller's software, we obtained a satisfactory impression of motor noise with remarkable noise reductions, 16 dB and 6 dB for the inrunner motor and outrunner motor, respectively. As a result, the operating noise at rider's ear location was below 60 dB and fulfilled the expectations of most cyclists.

Keywords: noise, bicycle, electric drive, permanent magnet motor

1 Introduction

Performance and ride quality are essential considerations for electric bicycles. With a motor, a motor drive and a battery to offer auxiliary propulsion during riding, electrically power assisted bicycles can be riding efforts saving. For most cyclists, low riding noise of electric bicycles is an intrinsic expectation. Nevertheless, motors are inherently associated with electromagnetic noise from the viewpoint of acoustics, mechatronics and literatures [1-5]. Their sound levels and performance are determined by structural designs, electromagnetic designs, motor drive schemes and manufacturing qualities. The axial-flux permanent magnet (AFPM) motors have certain advantages, such as high torque density,

smaller size and higher efficiency, over conventional radial-flux permanent magnet motors in various applications [6]. In this study, two types of conventional bicycles were modified and each equipped with a single-sided AFPM motor. Although with same pole and slot combination, one motor was constructed with inrunner design, and the other was outrunner design. These two electric bicycle prototypes exhibited different acoustic characteristics and noise issues during evolving designs.

To solve the noise problems systematically, we first examined the correlation between motor's construction and characteristics of motor drive. Acoustic cause analysis for potential noise sources was explored. Noise and vibration tests were performed with phase currents acquired. By analyzing time signature, spectrum or cepstrum data or both, we identified the noise and vibration causes for two motors. Finally, feasible noise countermeasures for both motor constructions were discussed and validated. For the inrunner motor, a 16 dB noise reduction was realized by applying sinusoidal pulse-width-modulation (PWM) drive comparing to the original square-wave PWM drive. For the outrunner motor, maximum noise reduction of 6 dB was achieved by refining its controller's software. Accordingly, the operating noise at rider's ear location of two motors was below 60 dB, and it fulfilled the expectations of most cyclists.

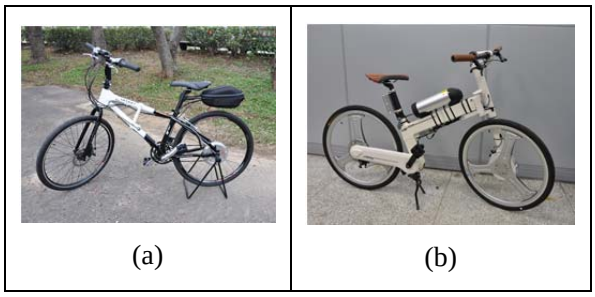

(a) (b)

Figure 1: Electric bicycle prototypes with single-sided AFPM motors: (a) inrunner motor and side-mounted at rear wheel hub; (b) outrunner motor and mounted at front wheel hub

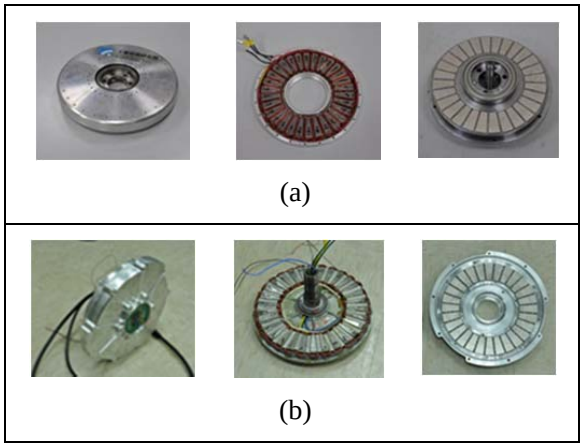

(a)

(b)

Figure 2: Single-sided AFPM motors: (a) inrunner design; (b) outrunner design

2 Motor Configurations and Analysis Methodology

2.1 Motor configurations

The major construction of single-sided AFPM motors in this study consists of a stator with windings, a rotor with permanent magnets, bearings, a shaft and housing. A motor drive, consisting of a power electronic converter and the associated controller, coordinates with the motor and the battery power.

Depending on the styling and the mounting location in a bicycle, the motor is constructed either as an inrunner or an outrunner design based on the structure of the rotor. Two electric bicycle prototypes of this study are shown in Fig. 1. Their developing motors were realized as pancake shape structures for slim look. These two motors, the stators and the rotors are shown in Figs. 2a and 2b. Table 1 shows the product profile of the propulsion system studied.

Table 1: Product profile of the propulsion system studied

	Item	Specification
Electric motor	Type	AFPM (gearless)
	Construction	Inrunner;Outrunner
	Maximum power	250 W
	Number of phases	3
	Number of poles	28
	Number of slots	30
	Bearing	Ball bearing
Controller	PWM switching (inrunner motor)	20 kHz
	PWM switching (outrunner motor)	10 kHz
Battery	Lithium-ion (inrunner motor)	24V/10Ah
	Lithium-ion (outrunner motor)	36V/12Ah

2.2 Acoustic cause analysis methodology

The ability to achieve a good acoustic behavior, whatever the sources, is reducing the excitation forces and tailoring the system characteristics. Therefore, the details of electromagnetic and mechanical designs are important for acoustic behavior. For reducing emitted motor noise, we can control the excitation sources, isolate noise transfer paths or tailor structural dynamic behaviors.

In general, the normal component of the electromagnetic force and torque ripple are the main electromagnetic sources of noise and vibration. For electromagnetic force, Maxwell's stress tensor method is generally used and relates with the flux density in the air-gap [7]. Magnet configuration, air-gap length, slot dimensions as well as the number of the pole and slot combination have significant effects on the air-gap flux density distribution and therefore have influence on the electromagnetic forces. On the other hand, the torque produced by a brushless permanent magnet motor is a sum of reluctance torque, cogging torque and mutual torque [8]. Of the three torque terms, reluctance torque and cogging torque are usually undesired parasitic. These torque terms contain harmonics which lead to torque ripples. Minimizing these ripples is important in the design of permanent magnet motors.

To identify motor noise sources, it is essential to correlate the dominant acoustic frequencies with the electromagnetic and structural characteristics of a motor. In electric motors, the relationship between electrical and mechanical frequency as well as the pole and slot combination are significant for frequency investigation. For a permanent magnet motor given pole number of N_p and stator slot number of N_s, the fundamental frequency of the current in each phase is $(N_p/2)f_m$ or f_e, where f_e is the fundamental electrical frequency and f_m is the mechanical frequency [8]. For electromagnetic force in normal direction, $2f_e$ is its fundamental frequency [4]. In addition, the fundamental frequency of torque ripple induced by tangential force harmonics, generated by six changes in the rate of change of flux, can be determined from $6f_e$ for brushless DC motors [2, 4]. The fundamental frequency of cogging torque, due to the interaction between the permanent magnets of the rotor and the stator slots or teeth independent of any current, is the least common multiple of the number of pole and slot multiplied by f_m [1].

In this study, the motor drive, the motor structure as well as the characteristics of vibration and emitted noise are crucial for resolving acoustic issues. The measured data included phase currents, rotor position, rotor speed, motor vibration and emitted noise. Depending on the acoustic issue, time signature, spectrum or cepstrum data or both were analyzed; further modal testing was performed on the outrunner motor as structural resonance occurred.

3 Investigation and Reduction of Noise for Inrunner Motor

3.1 Acoustic assessment and cause analysis

For the electric bicycle shown in Fig. 1a, its motor is mounted at the side of rear wheel hub. With square-wave PWM drive, this brushless DC motor exhibited a 72 dB operating noise at rider's ear location under full load condition. The influence of PWM was firstly excluded because the switching frequency of 20 kHz is in the upper bound of audible hearing range. For correlation analysis among noise, vibration and motor drive, this study measured the near-field noise at 10 cm distance and far-field noise at 1 m distance away from the motor's housing, noise at rider's ear height, vibration of motor's housing and phase currents. Figure 3 illustrates the test setup at a hemi-anechoic chamber.

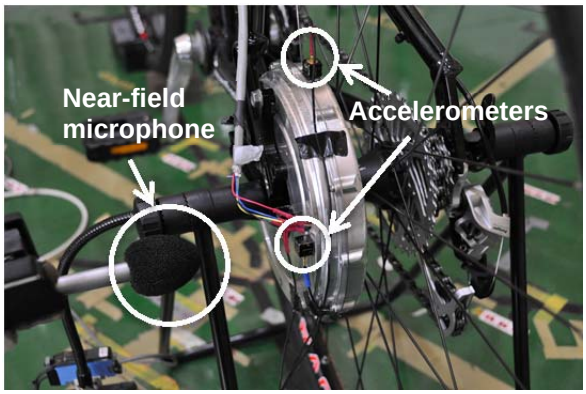

Figure 3: Test setup of electric bicycle equipped with an inrunner motor

Figure 4 shows motor's U-phase current and axial vibration measured on the motor's housing at full load condition, operating at 181 rpm. Given a rotor of 28 poles, the measured phase current has 14 electrical cycles in one complete revolution of rotor. Measured axial average vibration level was

74 m/s^2 with the maximum being 90 m/s^2, whereas the radial vibration was 10 m/s^2 in average and can be neglected. Since the noise concern happened both at full load and at no load conditions, this paper only illustrates the no load condition for noise source identification thereafter. Further spectrum analysis of noise and vibration shown in Fig. 5 revealed that the major frequencies correlated well and dominated at 168, 505, 1010 and 1515 Hz.

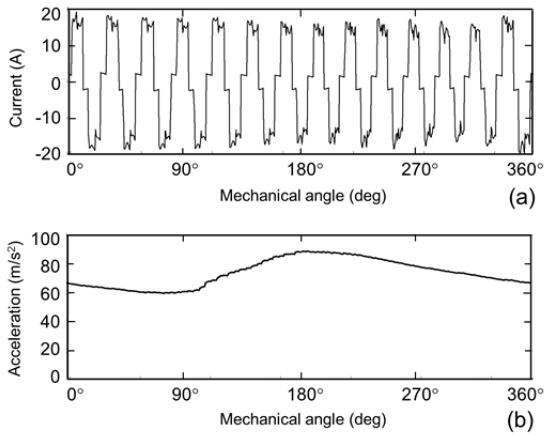

Figure 4: Time signatures for motor drive with square-wave PWM at full load and 181 rpm: (a) current of U-phase; (b) vibration of the motor's housing

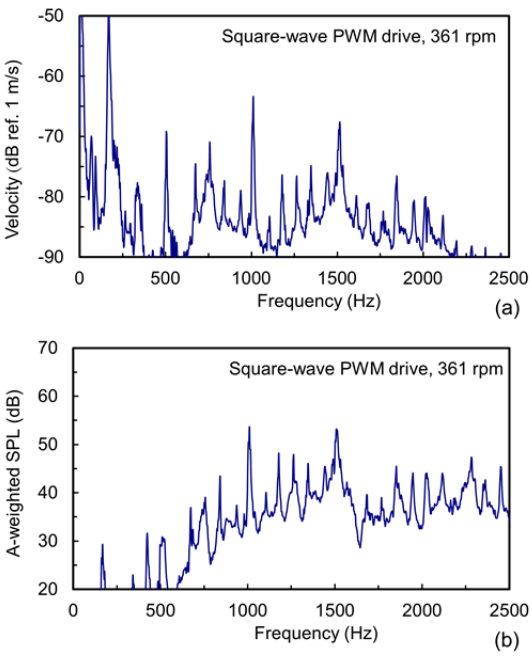

Figure 5: Spectrum analysis for motor drive with square-wave PWM at no load and 361 rpm: (a) vibration of the motor's housing; (b) motor noise at 1 m distance

Recalling the pole number being 28 and the motor speed being 361 rpm, the fundamental electrical frequency, f_e, was 84.2 Hz. Therefore, the fundamental frequency of torque ripple caused by tangential force harmonics is $6f_e$ which was 505 Hz. As a result, aforementioned vibration and noise peaks are located at frequencies of $2f_e$, $6f_e$, $12f_e$ and $18f_e$. In other words, the torque ripple was the root cause, which resulted in vibration of the motor's housing and consequent noise emission.

3.2 Noise reduction and validation

The high operating noise was related with the tangential force harmonics because of current control scheme. Instead of using square-wave PWM drive, the motor drive was modified as sinusoidal PWM. Figure 6 shows the time signatures of U-phase current and the vibration of motor's housing in one rotor revolution at full load condition and 180 rpm. The vibration measured at the motor's housing reduced dramatically to 11 m/s^2, which was only 15% of the one with square-wave PWM drive.

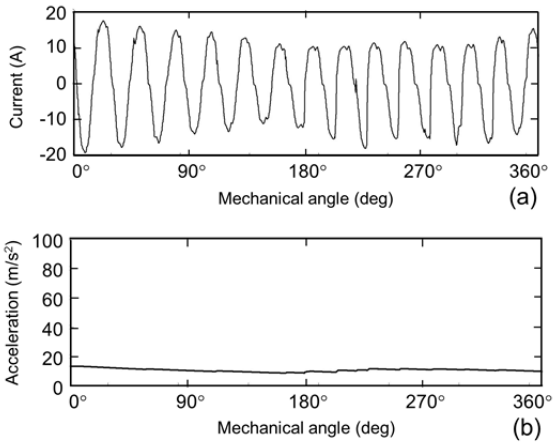

Figure 6: Time signatures for motor drive with sinusoidal PWM at full load and 180 rpm: (a) current of U-phase; (b) vibration of the motor's housing

Figure 7 compares the emitted noise for different PWM methods under different load conditions. By using sinusoidal PWM, the motor noise measured at 1 m distance away from the motor's housing reduced 15.5 and 3.6 dB at full load and no load condition, respectively; noise measured at rider's ear location also reduced 14.4 and 4 dB at full load and no load condition, respectively.

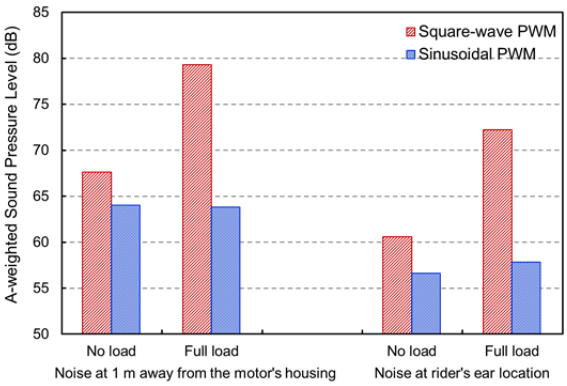

Figure 7: Comparison of emitted noise for different PWM methods under different load conditions

4 Investigation and Reduction of Noise for Outrunner Motor

4.1 Acoustic assessment and cause analysis

To pursue an attractive bicycle style, a study associated with an outrunner AFPM motor was conducted. It was based on the same pole and slot combination as the aforementioned inrunner motor. To keep a similar torque density with similar aspect ratio, the ball bearings were shrunk to smaller ones. The consequence was the smaller bearings had to counteract with the large axial force that exerted on the stator by the rotor magnets. Such a structure was prone to vibration under the magnetic force.

There are four assistance levels for the electrically power assisted bicycle prototype. With sinusoidal PWM drive, this motor exhibited a 59 dB and a 62 dB operating noise at 1 m distance away from the motor's housing for assistance level 3 and level 4, respectively. This operating noise was noticeable. Since the noise concern happened both at part load and at no load conditions, this paper only illustrates the analysis results at no load condition thereafter.

The bicycle was laid on the floor upside down for no load noise source identification. Similar as the inrunner motor case described in Sec. 3.1, this study also examined the synchronized data of vibration, noise, motor speed, phase currents and rotor position to identify the noise source. Figure 8 shows the test setup for measuring noise and vibration. The measurement included three microphones at far-field and near-field, an accelerometer at the mounting screw of the motor, currents of U, V and W phases as well as the rotor position.

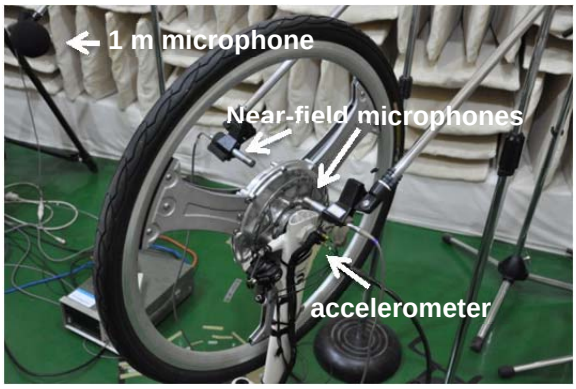

Figure 8: Noise and vibration measurement setup

To trace the dominant frequencies that contributed to noise source, Fig. 9 shows the spectrum of motor noise measured at 1 m distance away from the motor's housing and the axial vibration of the baseline motor for assistance level 3, operating at 270 rpm. It illustrated that the major frequencies were below 2 kHz; noise peaks were at 433, 507 and 806 Hz; vibration peaks were at 126, 433, 507 Hz and around 10 kHz. Similar characteristics were also seen for assistance level 4. The frequencies between noise and axial vibration correlated well and there was no perceptible PWM switching noise.

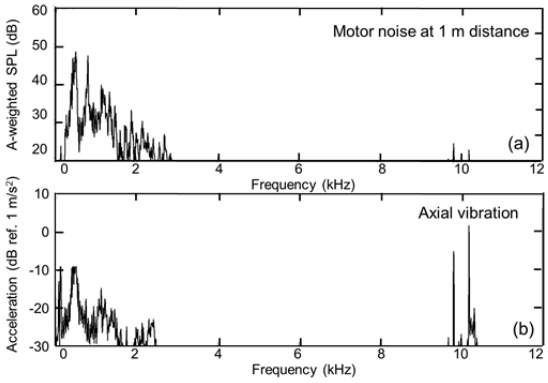

Figure 9: Spectrum for the outrunner motor at no load and 270 rpm: (a) motor noise at 1 m distance; (b) axial vibration

The 10 kHz vibration peak in Fig. 9 was clearly attributed to PWM switching frequency. The other noise and vibration peaks in Fig. 9, however, required further investigations. Referring to Sec. 2.2, for a 28-pole and 30-slot motor running at 270 rpm, the fundamental frequency of cogging torque is $420f_m$, 1890 Hz. It is concluded that the effect of cogging torque on the noise and vibration for this motor was negligible. The fundamental frequency of torque ripple induced by tangential force

harmonics is $6f_e$, 378 Hz, which was also not distinct in Fig. 9. The fundamental frequency of the axial electromagnetic force is $2f_e$, 126 Hz, which was noticeable at vibration but can be ignored for emitted noise after A-weighting.

Regarding the operating noise characteristics, the spectrum of motor noise usually consists of harmonic families. In practice, cepstrum analysis makes it easier to find these different harmonic families and the individual families can be used to identify the sources. Figure 10 shows the cepstrum of motor noise and axial vibration for assistance level 3, operating at 270 rpm. The corresponding f_m was 4.5 Hz. For motor noise, a primary rahmonic family with spacing of 7.44 ms, corresponding to the 135 Hz harmonic family, was identified. It was equivalent to $30f_m$. Recalling the number of stator slots is 30, it is concluded that the operating noise of this motor was mainly attributed to the permeance variations due to the stator slotting effect. In other words, slotting breaks up the uniformity of the air gap and produces the periodic variation and harmonics in the air gap permeance wave [5]. In addition, there were secondary rahmonic families with spacings of 7.96 and 15.8 ms, corresponding to the 126 and 63 Hz harmonic families, respectively.

For axial vibration, two major rahmonic families with spacings of 7.96 and 15.8 ms, corresponding to two harmonic families 126 and 63 Hz, were identified. The 126 Hz harmonic family was $28f_m$, which was caused by axial electromagnetic force; whereas the 63 Hz harmonic family was $14f_m$, which was the electrical fundamental frequency f_e. Similar results were also obtained for assistance level 4.

To account for the proximity of the force harmonics to any resonant frequency, this study further executed an experimental modal testing of motor. Figure 11 shows the frequency response function measured at driving point of the motor's housing. These natural frequencies were at 233, 314, 430, 464 and 588 Hz. As a result, frequency of noise and vibration at 433 Hz which coincided with natural frequency of the structure made such a motor construction resonant and generated high operating noise and vibration accordingly.

The structural resonance at 430 Hz can be avoided either by changing the operating speed or stiffening the motor's housing. However, an easier and promising way was to refine the current waveform via controller's software.

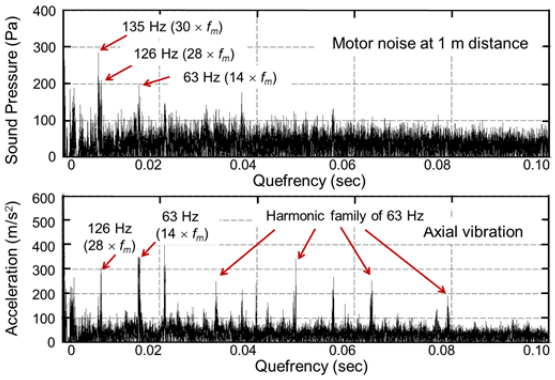

Figure 10: Cepstrum of motor noise and axial vibration for assistance level 3, operating at 270 rpm

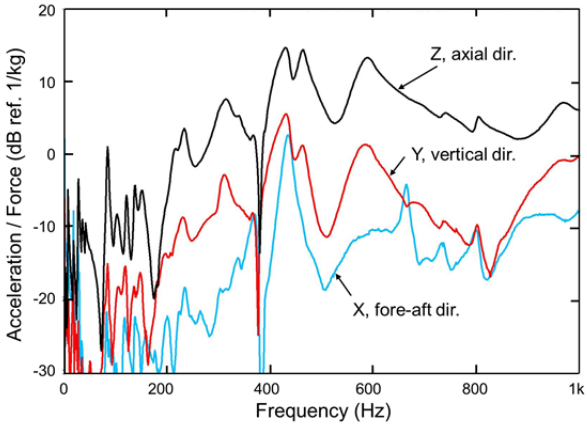

Figure 11: Frequency response functions measured at driving point of the motor's housing

4.2 Noise reduction and validation

To reduce the axial vibration and thus emitted noise, further refinement on the controller's software was implemented to improve the waveforms of phase currents. Figure 12 compares the time domain data in one rotor's rotation between the motor drive with original and with refined software. The data includes phase currents in the upper diagram and motor noise at 1 m distance in the lower diagram. As seen in Fig. 12, a smoother phase current waveforms and less noise was obtained for the motor drive with refined software. Figure 13 shows the effect of refined software on the motor noise at 1 m distance. Compared with the original software, a 6 dB noise reduction was obtained with the refined software for assistance level 1 and level 2; there was also a 5 dB and a 3 dB noise reduction for assistance level 3 and level 4, respectively. By using the motor drive with refined software, we obtained a satisfactory impression of motor noise. In addition,

the maximum motor noise at 1 m distance was also reduced from 62 dB to below 60 dB.

Since PWM method definitely changes the waveforms of phase currents so as it changes the noise behavior. Therefore, this study also investigated the influence of PWM switching frequency on the motor noise. Figure 14 compares the spectrum of motor noise at 1 m distance for refined motor drive with three PWM switching frequencies—8 kHz, 10 kHz and 20 kHz for assistance level 3. Apparently, there was no prominent PWM switching noise for 10 kHz and 20 kHz switching frequency. Figure 14a, however, clearly revealed that the 8 kHz PWM switching frequency caused severe switching noise associated with additional 2 kHz noise, although the switching loss became less. It needs a trade-off study between PWM switching noise and PWM switching loss for automotive industry.

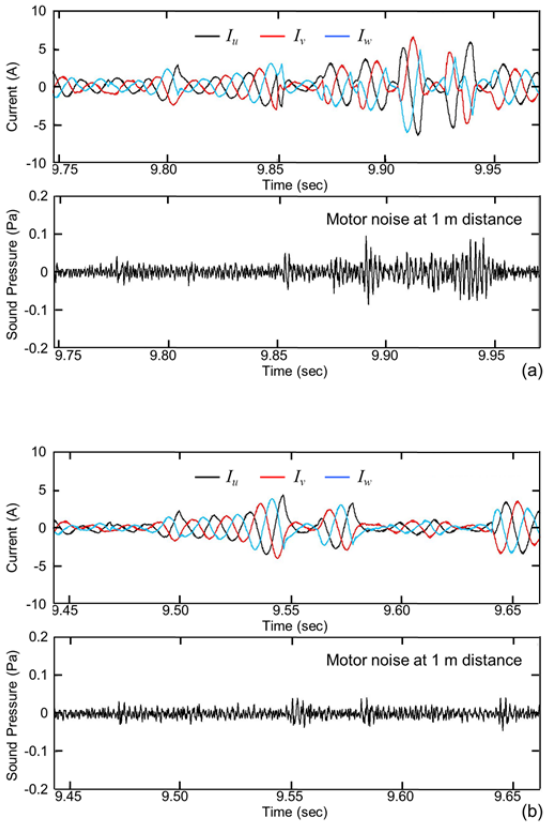

Figure 12: Comparison of phase currents and the corresponding motor noise in one rotor's rotation for assistance level 3: (a) motor drive with original software; (b) motor drive with refined software

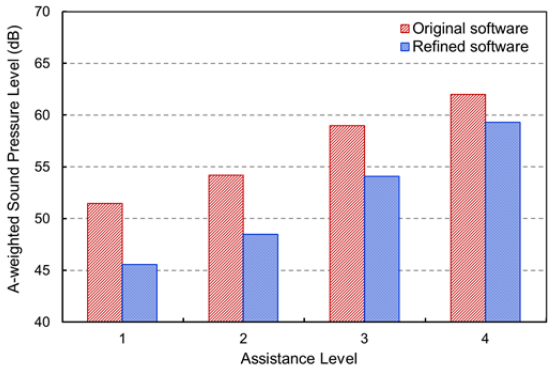

Figure 13: Comparison of motor overall noise at 1 m distance for controller with original software and with refined software

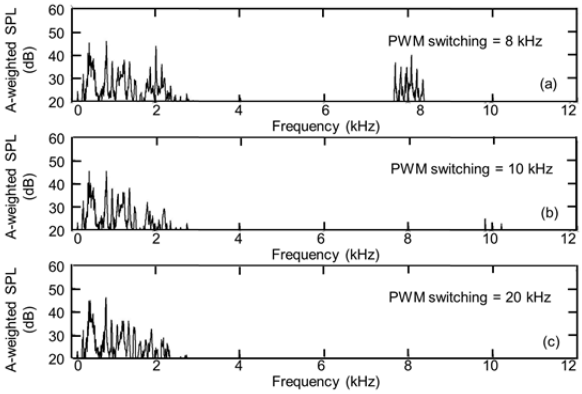

Figure 14: Spectrum of motor noise at 1 m distance for refined motor drive with different PWM switching frequencies for assistance level 3: (a) 8 kHz; (b) 10 kHz; (c) 20 kHz

5 Conclusions

Axial-flux permanent magnet motors are suitable for applications where slim look and high torque density are essential. Such a pancake shape construction, however, exhibits inherent structural weakness; motor's housing easily vibrates and emits noise if drive improperly. In this study, inrunner and outrunner AFPM motors under developing, caused noise concerns during riding. Through acoustic investigations both on the motor structure and the motor drive, associated with acoustic cause analyses in time domain, frequency domain or ceptstrum domain, the major vibration and noise peaks were correlated to their excitation sources.

The comprehensive noise source investigations illustrated that the root cause of inrunner motor noise in this study was the torque ripple induced by current control scheme. Whereas the cause of outrunner motor noise in this study was mainly

attributed to the stator slotting effect and the coincidence with structural resonance. In addition, the perceptibility of switching noise was highly linked to PWM switching frequency. Thus the motor drive scheme relating with current control and PWM switching frequency was a crucial attribute to the motor vibration and the emitted noise.

For the motors studied, a 16 dB noise reduction was realized by implementing sinusoidal PWM for the inrunner motor; a 6 dB noise reduction was achieved by refining the controller's software for the outrunner motor. As a result, the operating noise level at rider's ear location was below 60 dB and fulfilled the expectations of most cyclists.

Acknowledgments

The authors gratefully acknowledge the financial support of this project by the "Ministry of Economic Affairs" and "Mechanical and Systems Research Laboratories, ITRI" in Taiwan. Thanks are also due to the technical support team members Shih-Ming Lo, Pin-Yung Chen, Shao-Yu Li, Keng-Hung Lin, Chou-Zong Wu and Kou-Chang Hsiao for their assistances with the experiments.

References

[1] T. Sun et al., *Effect of pole and slot combination on noise and vibration in permanent magnet synchronous motor*, IEEE Transactions on Magnetics, ISSN 0018-9464, 47(5), (2011), 1038-1041

[2] M. Brackley and C. Pollock, *Analysis and reduction of acoustic noise from a brushless DC drive*, IEEE Transactions on Industry Applications, ISSN 0093-9994, 36(3), (2000), 772-777

[3] P. Vijayraghavan and R. Krishnan, *Noise in electric machines: a review*, IEEE Transactions on Industry Applications, ISSN 0093-9994, 35(5), (1999), 1007-1013

[4] J. H. Leong and Z. Q. Zhu, *Acoustic noise and vibration of direct-torque-controlled permanent magnet brushless DC drives*, Power Electronics, Machines and Drives Conference, E-ISBN 978-1-84919-616-1, (2012)

[5] S. Huang, M. Aydin and T. A. Lipo, *Electromagnetic vibration and noise assessment for surface mounted PM machines*, Power Engineering Society Summer Meeting, ISBN 0-7803-7173-9, (2001), 1417-1426

[6] M. Aydin, S. Huang, T.A. Lipo, *Axial flux permanent magnet disc machines: a review*, Wisconsin Electric Machines & Power Electronics Consortium, Research Report, (2004)

[7] R. Islam and I. Husain, *Analytical model for predicting noise and vibration in permanent-magnet synchronous motors*, IEEE Transactions on Industry Applications, ISSN 0093-9994, 46(6), (2010), 2346-2354

[8] D. Hanselman, *Brushless Permanent Magnet Motor Design* 2nd ed., ISBN 1-881855-15-5, Ohio, Magna Physics Publishing, 2006

Authors

Ming-Hung Lu is a senior researcher at Industrial Technology Research Institute (ITRI), Taiwan. He earned his B.S. and M.S. degrees in Mech. Eng. from the National Chiao-Tung Univ. in Taiwan. His research areas include noise and vibration development for powertrain, vehicle and EV infrastructures. He has published over 45 technical papers on his research.

Dr. Ming Une Jen is a senior researcher at ITRI. She received her Ph.D. degree in Mech. Eng. from the Univ. of Maryland. Her research areas include vehicle NVH engineering, EV infrastructures and chassis engineering. Dr. Jen has published over 50 technical papers concerning her research.